Laser & Photonics Reviews

LASER & PHOTONICS REVIEWS

www.lpr-journal.org

RESEARCH ARTICLE

Polarization-Controlled Tunable Beam Shift via Pancharatnam-Berry Phase Gradients in Photonic Crystal Slabs

Riwa Hao[1,2] | Jiale Chen[1,2] | Zi-xin Zhou[1,2] | Yan-qing Lu[1,3,4,5,6] | Jun-long Kou[1,2,5,6,7]

[1]School of Electronic Science and Engineering, Nanjing University, Nanjing, China | [2]School of Integrated Circuits, Nanjing University, Suzhou, China | [3]College of Engineering and Applied Sciences, Nanjing University, Nanjing, China | [4]National Laboratory of Solid-State Microstructures, Nanjing, China | [5]Key Laboratory of Intelligent Optical Sensing and Manipulation, Ministry of Education, Nanjing University, Nanjing, China | [6]Wujin-NJU Institute of Future Technology, Changzhou, China | [7]Jiangsu Key Laboratory of Semiconductor Laser and Sensing Technology, Suzhou, China

Correspondence: Yan-qing Lu (yqlu@nju.edu.cn) | Jun-long Kou (jlkou@nju.edu.cn)

Received: 9 September 2025 | **Revised:** 15 December 2025

Keywords: beam shift | photonic crystal slab | polarization singularities

ABSTRACT

When a light beam hits the interface between different media, the positions of the refracted and reflected beams deviate from those predicted by traditional geometric optics, resulting in beam shifts phenomenon. Beam shifts and manipulation technologies play an indispensable role in precision measurement, biochemical sensing, optical switching, and photodetection. Traditional beam shift phenomena, such as Goos-Hänchen shifts and Imbert-Fedorov shifts, typically require oblique incidence conditions, with the shift magnitudes often limited to the nanoscale, significantly constraining integration and reconfigurability. Moreover, these minute shifts are susceptible to environmental noise, making it challenging to meet the demands for large-range, high-sensitivity beam shifts. Photonic crystals offer strong light field manipulation capabilities and support a variety of polarization singularity configurations, including bound states in the continuum and circularly polarized singularities, providing a novel platform for the generation and control of beam shifts. This study leverages the geometric phase configuration to develop a multidimensional control framework for Imbert-Fedorov shifts based on photonic crystal slabs, achieving continuous tuning of beam shifts on the order of four wavelengths for a normal incident beam. This approach establishes a new paradigm for high-sensitivity optical sensing, beam manipulation, and reconfigurable photonic switching applications.

1 | Introduction

Beam shift phenomena are central to wave optics and spin-orbit interaction studies, encompassing Goos-Hänchen (G-H) shifts [1–5], the photonic spin Hall effect (PSHE) [6, 7] and Imbert-Fedorov (I-F) shifts [8–10]. These phenomena in various systems have garnered significant attention due to their intriguing physical mechanisms and potential applications [11–13]. The classical G-H shifts describe the shifts of a beam along the plane of incidence under total reflection, arising from the phase gradient of Fresnel coefficients. In contrast, the I-F shifts manifest as transverse shifts perpendicular to the plane of incidence for circularly polarized light during reflection or refraction, driven by the geometric phase due to spin-orbit angular momentum coupling [14–16]. The PSHE extends the concept to spin-locked splitting, achieving wavelength-scale lateral separation by imposing opposite Pancharatnam-Berry (PB) phases on the left-handed and right-handed spin components via interfaces or metasurfaces [17]. Additionally, exotic shift phenomena based on topological boundary states or non-conventional

beams reveal richer momentum reconfiguration and topologically protected characteristics. Despite considerable theoretical and experimental progress in the study of optical beam shifts, several critical challenges persist. First, conventional interfaces or metasurfaces typically produce only nanoscale displacements—far smaller than the beam waist or wavelength—which severely restricts both experimental observability and practical utility. Second, the generation of such shifts generally requires oblique incidence, inevitably altering the beam propagation direction and complicating device integration. Moreover, the magnitude of conventional beam shifts is either difficult to tune or exhibits an extremely limited tuning range, which significantly hinders flexible beam manipulation in integrated photonic systems.

2D photonic crystal slabs (PCSs), as versatile platforms, have been extensively utilized for engineering optical fields in momentum space [18–20], enabling the generation of various far-field polarization singularities [21, 22], such as vortex points (V-points) [23–27] and circularly polarized points (C-points) [28–34]. In this study, we exploit the breaking of in-plane symmetry to transform V-point into C-points, demonstrating a PCS design that enables momentum-space phase engineering [35]. The PB phase gradients near Γ point exhibits linear distribution in momentum space, facilitating continuous, tunable I-F shifts on the order of wavelengths under normal incidence.

We investigate beam shifts using a versatile PCS platform composed of an amorphous silicon (α-Si) square lattice, focusing on the role of C-points. For the pristine PCS system with C_{4v} symmetry, the far-field polarization field strictly adheres to this symmetry. We select the polarization field corresponding to the irreducible representation A_2, which exhibits a topological charge of +1 on the TE_2 band of our choice. By transforming the square air-hole morphology into an isosceles triangular structure, we introduce in-plane C_2 symmetry breaking, retaining only a single mirror symmetry axis. The band structures before and after symmetry breaking are shown in Figure 1a. We select the transverse electric (TE_2) mode band and compute its far-field polarization distribution (Figure 1b), revealing a pair of C-points with opposite chirality along the k_x axis and a L-line near the Γ point exhibiting purely horizontal polarization. From the polarization angle distribution in momentum space (Figure 1c), two phase singularities with a π rotation correspond to C-points with a topological charge of 1/2. This C-point configuration induces a linear geometric phase near the Γ point, enabling I-F shifts of cross-polarized beams under normal incidence (Figure 1d). Figure 1e presents the Scanning electron microscope (SEM) image of the structure. The shifts exhibit a hyperbolic dependence on the incident polarization angle ϕ (Figure 1f): it reaches a minimum at ±45°, diverges as ϕ approaches 0° or 90°, and positive or negative polarization angles yield equal-magnitude shifts in opposite directions.

2 | Results

2.1 | Relationship between PB Phase Gradient and Beam Shifts

The quantitative relationship between beam shifts and phase gradient originates from the modulation of wavefront distribution by the geometric phase. Consider a Gaussian beam normally incident along z-axis, with its momentum-space distribution given by:

$$E_{in}(k_x, k_y) = E_0 \exp\left(-\frac{k_x^2 + k_y^2}{k_d^2}\right) \tag{1}$$

where k_x, k_y are the in-plane wavevector components, and k_d is the wavevector corresponding to the divergence angle. When a photonic crystal introduces a linear PB phase gradient along the k_x-direction, the phase is given by $\Phi_{PB}(k_x) = (\nabla_k \Phi)k_x$, where $\nabla_k \Phi = \frac{\partial \Phi}{\partial k_x}$. The output light field after phase modulation is:

$$E_{out}(k_x, k_y) = E_{in}(k_x, k_y) \exp\left[i\Phi_{PB}(k_x)\right] \tag{2}$$

According to the Fourier transform relationship, the real-space electric field is obtained via the inverse transform from momentum space. Using the stationary phase approximation, the extremum position is found to be $x = -\frac{\partial \Phi_{PB}}{\partial k_x}$. Accounting for the conversion from momentum space to real space, the I-F shifts are:

$$X_{IFS} = -\frac{\lambda}{4\pi} \nabla_k \Phi \tag{3}$$

This result can also be derived from the first moment of the light intensity in real space, as detailed in Section SI.

2.2 | Simulation Results and Discussion

PCSs provide an effective platform for realizing momentum-space phase gradients. Within the light cone, radiative resonant modes of a PCS corresponding to different plane-wave vectors couple with free-space plane waves, partially converting incident beam components with a specific polarization state into an orthogonal polarization state. Beyond resonance-induced phase changes, this conversion imparts a wavevector-dependent PB phase to the cross-polarized output components. When the incident and analyzed output polarization states are orthogonal, the PB phase variation is governed by the eigenmodes of the PCS, enabling different geometric phases through engineering the eigenpolarization field and controlling the incident polarization state. Using temporal coupled-mode theory (TCMT) [36–38], we analytically derive the geometric phase in cross-polarization conversion from the eigen-polarization field distribution of the photonic crystal. The derivation of the geometric phase is provided in Section SII.

$$\Delta\Phi_{PB} = \mp\left[\arg\left(S_3 + i(S_1 \sin 2\phi - S_2 \cos 2\phi)\right) - \frac{\pi}{2}\right] \tag{4}$$

here, ϕ denotes the angle between the incident light and the x-axis, which we define as the direction of symmetry breaking in the photonic crystal, while S_1, S_2, and S_3 represent the Stokes parameters of the eigenmode polarization field. Using a finite-element method (FEM) solver, the transmission and reflection responses of the studied PCS were computed for various linearly polarized incident conditions. Figure 2a shows the angle-resolved transmission spectra for different incident

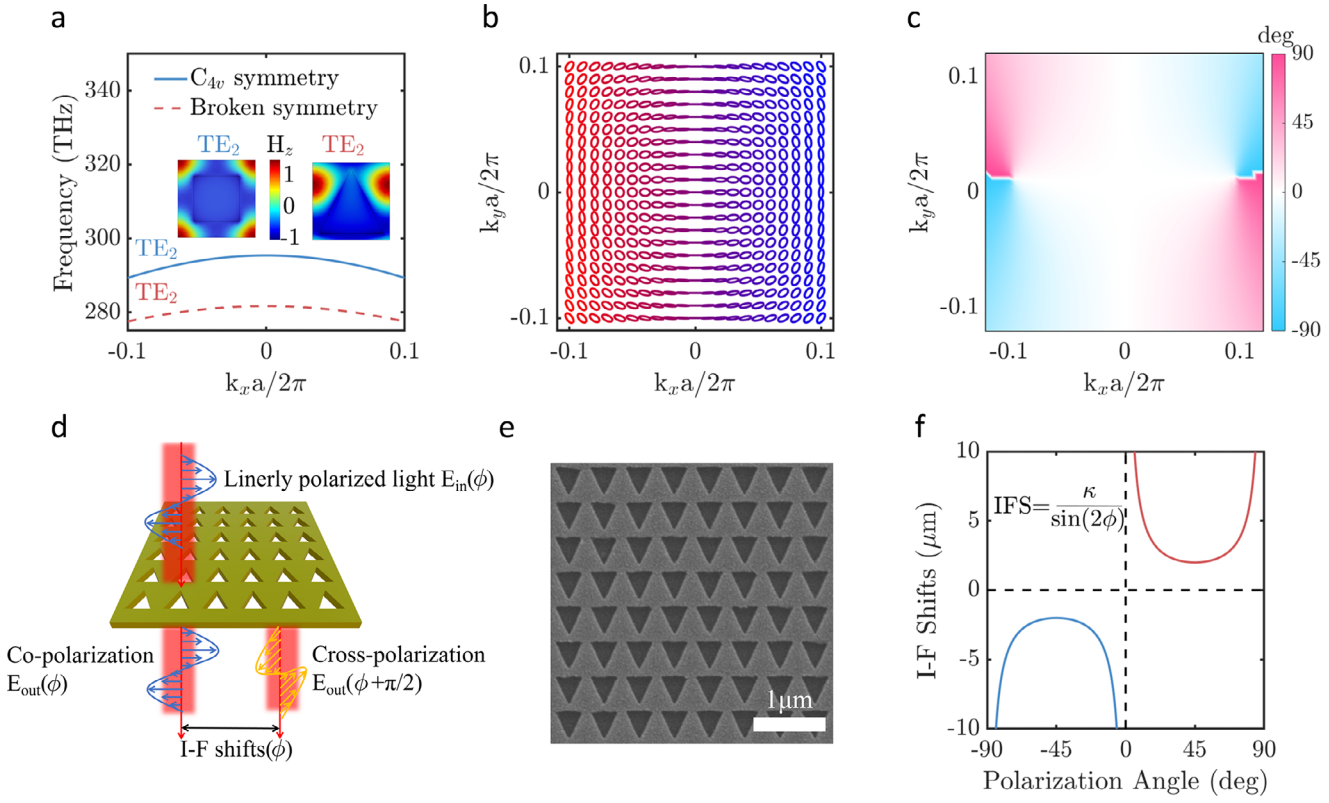

FIGURE 1 | Photonic crystal structure design supporting C-points and beam shifts. (a) Band structures before and after symmetry breaking. (b,c) Far-field polarization distribution and polarization angle distribution in momentum space after breaking in-plane C_2 symmetry. (d) Schematic of I-F shifts based on the PCSs. (e) SEM image of the sample surface. (f) Theoretical prediction of I-F shifts as a function of incident light polarization angle ϕ.

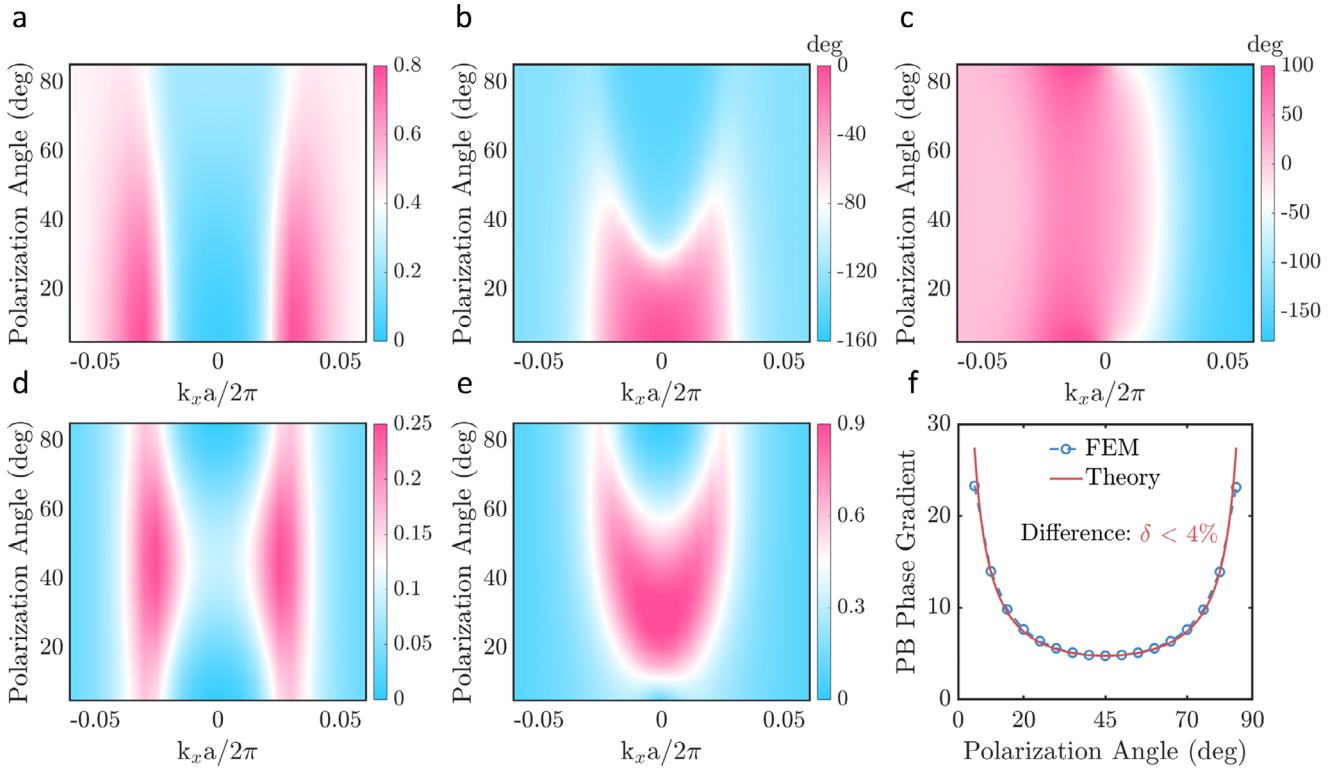

FIGURE 2 | Transmission, reflection response and PB phase distribution of photonic crystals under different incident linear polarization angles. (a) Total transmittance distribution. (b,c) Phase distributions of the co-polarized and cross-polarized components of the transmitted light. (d) Transmittance of the cross-polarized component. (e) Polarization conversion efficiency. (f) PB phase gradient calculated using theoretical models and FEM simulations.

linear polarization angles ϕ. The phase distribution of the co-polarized component, presented in Figure 2b, is symmetric about the Γ point with a PB phase gradient of zero, resulting in no beam shifts. In contrast, the phase distribution of the cross-polarized component, shown in Figure 2c, exhibits an asymmetric profile about the Γ point with a near-linear distribution near Γ point, driving significant beam shifts, with symmetry about $\phi = 45°$ and maximum phase gradients at $\phi = 0°$ and 90°. As shown in Figure 2d, the distribution of cross-polarization transmittance T_2 exhibits a maximum value of 25% at an incident polarization angle of $\phi = 45°$. Similarly, Figure 2e presents the distribution of polarization conversion efficiency η, which reaches a peak value exceeding 90%, demonstrating strong beam cross-polarization conversion driven by guided-mode resonance. By extracting the geometric phase gradient of the wavevector at the Γ point under different polarization angles ϕ, the I-F shifts curve obtained from FEM simulations show near-perfect agreement with theoretical predictions, with a maximum relative error of less than 4% (Figure 2f).

The propagation and shifts characteristics of a Gaussian beam through a PCS were simulated using the finite-difference time-domain (FDTD) method. Leveraging the hyperbolic symmetry of the system, we investigated incident polarization angles of $\phi = 0°$, 20°, and 45°. Simulations were performed on a finite-sized sample consisting of a 100 × 100 unit cells, with a 1064 nm Gaussian beam normally incident at the sample's center ($x = y = 0\,\mu m$) and a beam divergence angle of 3.8°. The sample is positioned at the $z = 0\,\mu m$ plane, with a Gaussian beam incident normally from above along the negative z-axis, and the transmitted beam is observed at $z = -9\,\mu m$. Figure 3a shows the intensity distribution of the co-polarized component of the transmitted beam with the beam spot centered at the origin, identical to the incident beam, indicating no beam shifts. Figure 3b,c illustrate the normalized distribution of the cross-polarized component in the x-y plane and the x-z plane, respectively, where the PB phase gradient induces beam shifts in the transverse direction. At $\phi = 0°$ and 90°, no divergence occurs, as the finite divergence angle of the Gaussian beam in FDTD real-space propagation simulations and optical experiments prevents the theoretically predicted infinite shifts. At $\phi = 0°$ or 90°, the cross-polarized component forms two symmetrically positioned, equally intense Gaussian spots along the positive and negative x-directions, resulting in a pronounced beam splitting effect. Figure 3d shows the intensity distribution along the x-axis, revealing that the beam shifts decrease from $\phi = 0°$ to 45°. As ϕ approaches 0°, a secondary intensity peak emerges, growing in strength until, at $\phi = 0°$, two equally intense and equidistant split beams are formed.

2.3 | Experimental Results and Discussion

We fabricated PCS by patterning an 82 nm thick α-Si thin film on a SiO_2 substrate. The slab comprises 200 × 200 unit cells, with its symmetry engineered to break in-plane inversion while preserving a single mirror axis, enabling control over the momentum-space polarization structure. The target wavelength of 1064 nm was selected to excite resonant modes that induce geometric phase gradients. Employing a real-space imaging system, we directly observed polarization-controlled transverse beam shifts and beam splitting, manifestation of the engineered momentum-space phase distribution.

The experimental configuration, depicted in Figure 4a, facilitates precise control of the incident beam polarization and divergence. A laser beam is first collimated and its divergence angle adjusted via a 4f optical system. The beam is then directed normally onto the PCS surface through an objective lens. Linear polarizers, positioned on either side of the sample plane and oriented orthogonally, regulate the incident polarization and analyze the emergent light. The in-plane wavevector $k_{\parallel}$, tied to the divergence angle, is tailored in Fourier space by adjusting the aperture size before the focusing lens. The Gaussian beam exhibits a waist radius of approximately 3 μm. The beam boundary is defined as the position at which the intensity decays to 1/e of its maximum value. Post-polarization analysis, the beam is imaged onto a CCD camera using a focusing lens, with a broadband light source facilitating spot localization.

To establish a reference, an unstructured α-Si window, matching the PCS 82 nm thickness, is initially placed in the sample plane. The finite extinction ratio of polarizers permits minimal transmission of co-polarized light, enabling identification of the original beam position and coordinate origin. Replacing the window with the PCS, we measured the normalized intensities of cross-polarized and co-polarized beams, as shown in Figure 4b, c. Transverse beam shifts, consistent with theoretical predictions driven by momentum-space phase gradients, were directly observed. The shifts magnitude, approximately 2 μm as determined by tracking the beam center, approaches the beam waist radius. Additionally, at incident polarization angles of 0° or 90°, beam splitting into two symmetric spots along the $+x$ and $-x$ directions was observed (Figure 4d, e), reflecting the symmetry-induced phase engineering of PCS.

The relationship between beam shifts and incident polarization angle, illustrated in Figure 4f, follows a theoretical framework where an ideal plane wave at the Γ point yields a shifts governed by:

$$\frac{\partial \Phi_{PB}}{\partial k_x} = \frac{\kappa}{\sin 2\phi} \tag{5}$$

with κ denoting the position of C-point. The physical significance of κ and the detailed derivation of the phase gradient are provided in Section SIII. At 0° and 90°, the model predicts divergence; however, experimental shifts remain finite. This arises from the Gaussian beam's inherent divergence, distributing momentum near the Γ point and yielding a finite average phase gradient. Consequently, shifts approximate the beam waist radius, aligning with practical observations and the PCS nonlocal resonant effects. For the specific impact of the Gaussian beam's inherent divergence on the shifts, please refer to Section SIV. By tuning the linear polarization angle, we achieve precise and continuous control over the magnitude and direction of the shifts. Experimentally, we observe significant transverse shifts, approximately four times the wavelength, and beam splitting phenomena at specific polarization angles. Notably, the tunable range of the beam displacement is by no means limited to four wavelengths. By further adjusting the divergence angle of the incident Gaussian beam, the shift magnitude can be continuously extended

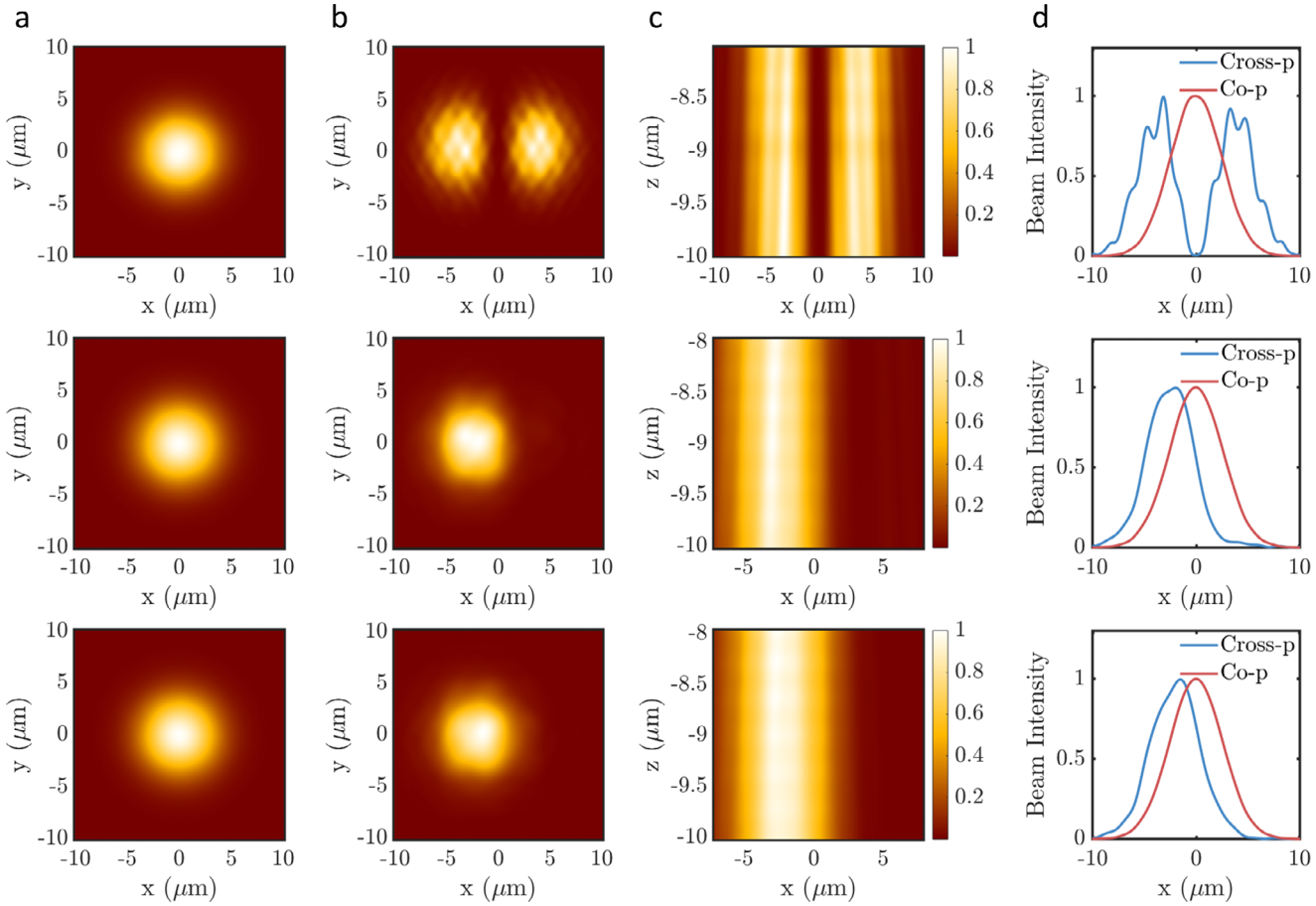

FIGURE 3 | Simulation results of the PCS applied to realize polarization-controlled lateral shifts. (a) Normalized intensity distribution of the co-polarized component of the emitted light at $z = -9\,\mu m$ for incident light polarization angles of 0°, 20° and 45°. (b) Normalized intensity distribution of the cross-polarized component of the emitted light. (c) Cross-sectional distribution of the cross-polarized component along the propagation direction ($y = 0\,\mu m$). (d) Normalized intensity distribution of the observed beam along the x-axis, extracted from (a) and (b) The blue and red lines represent the normalized intensity distributions of the cross-polarized and co-polarized components, respectively.

from 2 μm up to the scale of the Gaussian beam envelope itself—far exceeding the wavelength—while still relying solely on the incident polarization state as the single control knob. This purely polarization-driven, large-range tunability, combined with the strict normal-incidence geometry, is particularly advantageous for flexible beam manipulation in integrated photonic systems.

2.4 | Control of C-Points and Beam Shifts via Symmetry Breaking

Bound states in the continuum (BICs) are localized states coexisting with extended waves inside the continuous spectrum range, which have infinite lifetimes without any radiation. In this study, we investigate the manipulation of C-points and V-points within PCS by breaking the C_{4v} symmetry of the system. Initially, the V-point is located at the Γ point, representing symmetry-protected bound state in the continuum (BIC) with topological charge of 1. By introducing in-plane C_2 symmetry breaking, while preserving mirror symmetry along the y-axis, the V-point at the Γ point splits into two C-points along the $+x$ and $-x$ directions. These C-points are characterized by modes with opposite chirality: a left-handed (LH) C-point paired with a right-handed (RH) C-point. The separation between these C-points and the Γ point in momentum space can be precisely controlled by tuning the symmetry-breaking factor, denoted as α. The symmetry-breaking factor α is mathematically defined as $\alpha = \frac{l-l'}{l}$, where l denotes the length of the base of an isosceles trapezoid, l' represents the length of its top, and the height of the trapezoid is fixed at l. To isolate the effect of symmetry breaking, the area of the trapezoid is kept constant while α is varied. The parameter α ranges from 0 to 1: at $\alpha = 0$, the system retains its original C_{4v} symmetry (with the etched central region forming a square), whereas at $\alpha = 1$, the structure transitions into a triangular configuration. As α increases, the C-points exhibit progressive shifts from the Γ point in momentum space. In the regime of weak symmetry breaking, the geometric symmetry-breaking factor α serves as an effective first-order approximation for the dipole moment perturbation. In this linear regime, the perturbation term within d_x—defined as the x-component of the far-field polarization vector in momentum space—is linearly proportional to α, resulting in a linear scaling of the separation between the C-point and the Γ point as α increases. However, as α increases further, the error associated with the first-order approximation grows, and higher-order effects become significant, leading to a deviation from the linear region. For a detailed derivation

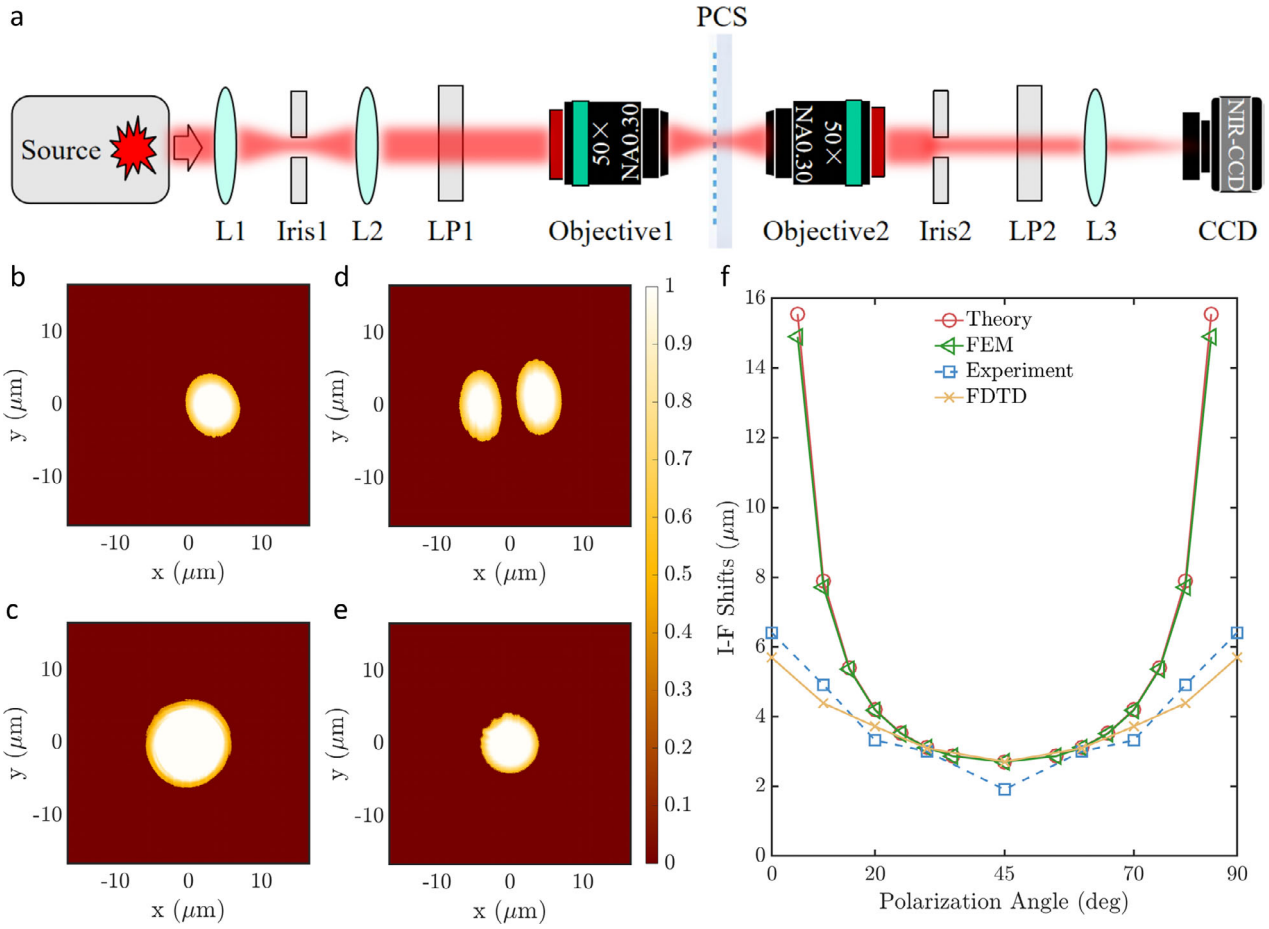

FIGURE 4 | Measurement of beam shifts controlled by incident polarization state. (a) Schematic of the experimental setup for real-space beam shifts measurements. (b, c) Normalized intensity distributions of cross-polarized and co-polarized emergent light at a 45 ° incident polarization angle. (d, e) Normalized intensity distributions of cross-polarized and co-polarized emergent light at a 0 ° incident polarization angle, exhibiting beam splitting. (f) Comparison of theoretical and experimental beam shifts across varying incident polarization angles.

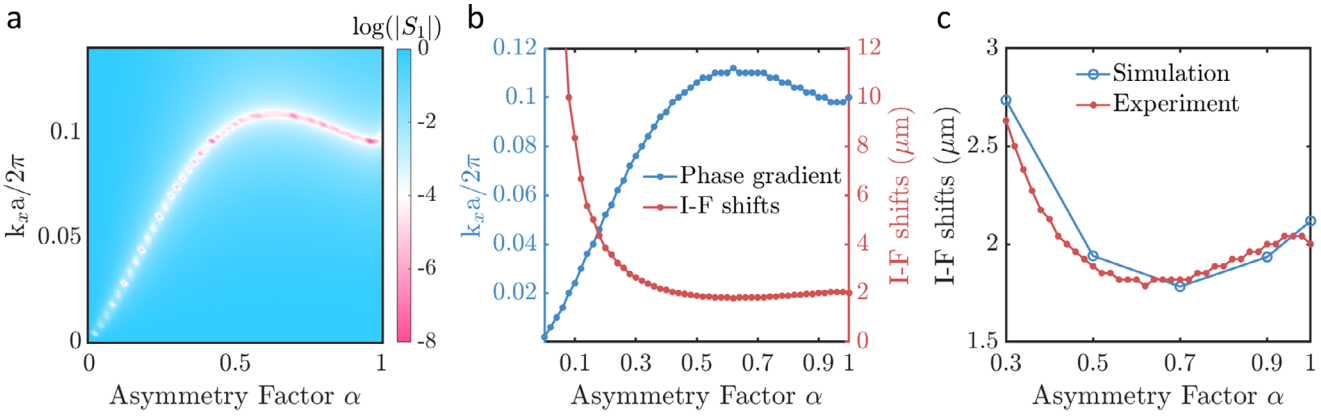

FIGURE 5 | The evolution of the position of C-point with respect to the value of the asymmetry factor. (a) The relationship between the position of the C-point and the asymmetry factor. (b) The evolution of the position of the C-point and beam shifts with respect to the asymmetry factor. (c) Experimental measurement of beam shifts as a function of the evolution of the asymmetry factor.

regarding the impact of α on the Stokes parameters and the resulting PB phase distribution, please refer to Section SIII.

To illustrate these effects, Figure 5a depicts the relationship between the positions of the C-points and the symmetry-breaking factor α following the disruption of C_{4v} symmetry. Theoretical analysis indicates that the distance between the C-points and the Γ point is inversely proportional to the phase gradient at the Γ point. Further, Figure 5b elucidates the dependence of beam shifts magnitude on α when the polarization angle of the incident light

is fixed at 45°. Finally, Figure 5c provides a comparative analysis of the theoretically predicted beam shifts against experimentally measured values. These findings underscore that the modulation of the symmetry-breaking factorα not only governs the spatial distribution of C-points in momentum space but also plays a pivotal role in determining the characteristics of beam shifts. Such insights are invaluable for advancing both theoretical frameworks and experimental methodologies in photonic crystal research.

3 | Conclusion

In conclusion, this study demonstrates a novel approach to achieve continuous tuning of beam displacement for normally incident light on the wavelength scale by controlling the polarization state of the incident light. At a wavelength of 1064 nm, we achieved beam displacements ranging from 2 μm to 6 μm, surpassing the beam spot radius. The displacement originates from the geometric phase induced by cross-polarization conversion in the guided-mode resonance of photonic crystal slabs. In contrast to traditional beam displacement techniques, our method enables arbitrary displacement at any position on the photonic crystal slab without altering the beam's propagation direction. Furthermore, the ability to adjust displacement magnitude solely through polarization state modulation provides new degrees of freedom for designing compact and reconfigurable optical systems, paving the way for applications in high-sensitivity optical sensing and photonic switching.

4 | Methods

4.1 | Theoretical Analysis

Please see the Supplementary Information for the detailed derivations and discussions.

4.2 | Numerical Simulations

Eigenmode simulations for the PCS structures in Figures 1, 2, and 4 are performed using a finite-element eigenfrequency solver. The simulations of the beam lateral shifts in Figure 3 were performed by the finite-difference time-domain method.

4.3 | Sample Fabrication

First, a homogeneous α-Si layer with a thickness of 82 nm was deposited onto a 500-μm-thick fused silica substrate using chemical vapor deposition (PECVD). Following pre-treatment with hexamethyldisilane (HMDS), the substrate undergoes spin-coating with a positive E-beam resist (AR-P200) that was 200-nm-thick. Subsequently, a water-soluble conductive polymer was applied to the E-beam resist layer to facilitate the removal of excess electrons during the E-beam writing process. The photonic crystal pattern was inscribed on the E-beam resist utilizing E-beam lithography (Elionix ELS-F125). Afterward, the conductive polymer was dissolved in water, and the resist undergoes development. Upon completion of this development phase, the pattern was transferred onto a 20-nm-thick chromium layer through electron beam evaporation (EBE) technology. The patterned chromium served as a hard mask for dry etching of the alpha-Si layer within a CHF_3 and SF_6 mixed plasma environment (ULVAC CE300I). Finally, the hard mask was removed using an ammonium cerium nitrate solution.

Author Contributions

R.H. and J.C. contributed equally to this work. J.-L.K. and J.C. conceived the idea. R.H. and J.C. developed the theoretical framework, performed simulations, conducted experiments, and analyzed the data with feedback from J.-L.K. and Y.-Q.L. Z.Z. prepared all the samples required for the experiments. All authors contributed to the manuscript preparation.

Acknowledgements

Riwa Hao and Jiale Chen contributed equally to this work. This work is supported by Advanced Materials-National Science and Technology Major Project (No. 2025ZD0615900); the National Key Research and Development Program of China (No. 2022YFA1405000); National Natural Science Foundation of China (No. T2488302); Natural Science Foundation of Jiangsu Province, Major Project (No. BK20243067); Leading-Edge Technology Program of the Jiangsu Natural Science Foundation (No. BK20232001); National Natural Science Fund for Excellent Young Scholars (Overseas); Fundamental Research Funds for the Central Universities; Nanjing University Integrated Research Platform of the Ministry of Education - Top Talents Program.

[Correction added on 27 January 2026, after first online publication: the Acknowledgment section was updated in this version.]

Conflicts of Interest

The authors declare no conflicts of interest.

Data Availability Statement

The data that support the findings of this study are available from the corresponding authors upon request.

Conflicts of Interest

The authors declare no conflict of interest.

References

1. F. Goos and H. Hänchen, "Ein Neuer und Fundamentaler Versuch Zur Totalreflexion," *Annalen der Physik* 436, no. 7–8 (1947): 333–346, https://onlinelibrary.wiley.com/doi/abs/10.1002/andp.19474360704.

2. X. Liu, Z. Liu, F. Zhou, et al., "Dual Quasi-Bound States in the Continuum and Their Enhanced Goos–Hänchen Shifts Based on the Waveguide Grating System," *Optics & Laser Technology* 187 (2025): 112817, https://www.sciencedirect.com/science/article/pii/S0030399225004086.

3. X. Yang, W. Liu, Z. Wei, et al., "Research on Dynamic Control of Goos–Hänchen Shifts of Dual-Band Beams Based on Quasi-Bound States in the Continuum," *Optics Communications* 585 (2025): 131841, https://www.sciencedirect.com/science/article/pii/S0030401825003694.

4. F. Wu, T. Liu, M. Luo, H. Li, and S. Xiao, "Giant Goos–Hänchen Shifts with High Reflection Driven by Fabry–Pérot Quasi-Bound States in the Continuum in Double-Layer Gratings," *Physical Review B* 109 (2024): 125411, https://link.aps.org/doi/10.1103/PhysRevB.109.125411.

5. Z. Zheng, Y. Zhu, J. Duan, M. Qin, F. Wu, and S. Xiao, "Enhancing Goos–Hänchen Shift Based on Magnetic Dipole Quasi-Bound States in the Continuum in All-Dielectric Metasurfaces," *Optics Express* 29, no. 18 (2021): 29541–29549, https://opg.optica.org/oe/abstract.cfm?URI=oe-29-18-29541.

6. M. Onoda, S. Murakami, and N. Lporaosa, "Hall Effect of Light," *Physical Review Letters* 93 (2004): 083901, https://link.aps.org/doi/10.1103/PhysRevLett.93.083901.

7. K. Y. Bliokh and Y. P. Bliokh, "Conservation of Angular Momentum, Transverse Shift, and Spin Hall Effect in Reflection and Refraction of an Electromagnetic Wave Packet," *Physical Review Letters* 96 (2006): 073903, https://link.aps.org/doi/10.1103/PhysRevLett.96.073903.

8. C. Imbert, "Calculation and Experimental Proof of the Transverse Shift Induced by Total Internal Reflection of a Circularly Polarized Light Beam," *Physical Review D* 5 (1972): 787–796, https://link.aps.org/doi/10.1103/PhysRevD.5.787.

9. O. Hosten and P. Kwiat, "Observation of the Spin Hall Effect of Light via Weak Measurements," *Science* 319, no. 5864 (2008): 787–790, https://www.science.org/doi/abs/10.1126/science.1152697.

10. Y. Qin, Y. Li, H. He, and Q. Gong, "Measurement of Spin Hall Effect of Reflected Light," *Optics Letters* 34, no. 17 (2009): 2551–2553, https://opg.optica.org/ol/abstract.cfm?URI=ol-34-17-2551.

11. M. Wei, Y. Long, F. Wu, G.-G. Liu, and B. Zhang, "Abrupt Lateral Beam Shifts from Terahertz Quasi-Bound States in the Continuum," *Science Bulletin* 70, no. 6 (2025): 882–888, https://www.sciencedirect.com/science/article/pii/S2095927325000192.

12. M. Kang, T. Liu, C. T. Chan, and M. Xiao, "Applications of Bound States in the Continuum in Photonics," *Nature Reviews Physics* 5, no. 11 (2023): 659–678, https://doi.org/10.1038/s42254-023-00642-8.

13. J. Wang, M. Zhao, W. Liu, et al., "Shifting Beams at Normal Incidence via Controlling Momentum-Space Geometric Phases," *Nature Communications* 12, no. 1 (2021): 6046, https://doi.org/10.1038/s41467-021-26406-5.

14. M. Onoda, S. Murakami, and N. Lporaosa, "Geometrical Aspects in Optical Wave-Packet Dynamics," *Physical Review E* 74 (2006): 066610, https://link.aps.org/doi/10.1103/PhysRevE.74.066610.

15. K. Y. Bliokh and Y. P. Bliokh, "Conservation of Angular Momentum, Transverse Shift, and Spin Hall Effect in Reflection and Refraction of an Electromagnetic Wave Packet," *Physical Review Letters* 96 (2006): 073903, https://link.aps.org/doi/10.1103/PhysRevLett.96.073903.

16. K. Y. Bliokh and A. Aiello, "Goos–Hänchen and Imbert–Fedorov Beam Shifts: An Overview," *Journal of Optics* 15, no. 1 (2013): 014001, https://dx.doi.org/10.1088/2040-8978/15/1/014001.

17. M.-Z. Chong, "Generation of Polarization-Multiplexed Terahertz Orbital Angular Momentum Combs via All-Silicon Metasurfaces," *Light: Advanced Manufacturing* 5, no. LAM2024020019 (2024): 400, https://www.light-am.com//article/id/655720f0-449e-492f-b0a9-2e5bfe8b8e00.

18. C. Guo, H. Wang, and S. Fan, "Squeeze Free Space with Nonlocal Flat Optics," *Optica* 7, no. 9 (2020): 1133–1138, https://opg.optica.org/optica/abstract.cfm?URI=optica-7-9-1133.

19. Y. Zhang, M. Zhao, J. Wang, et al., "Momentum-Space Imaging Spectroscopy for the Study of Nanophotonic Materials," *Science Bulletin* 66, no. 8 (2021): 824–838, https://www.sciencedirect.com/science/article/pii/S2095927320307581.

20. S. Zhang, M. Zong, Y. Liu, et al., "Universal Polarization- and Angle-Independent Quasi-Bound States in the Continuum via Degeneracy Protection in Metasurfaces," *Laser & Photonics Reviews* 19, no. 23 (2025): e00859, https://onlinelibrary.wiley.com/doi/abs/10.1002/lpor.202500859.

21. A. Chen, W. Liu, Y. Zhang, et al., "Observing Vortex Polarization Singularities at Optical Band Degeneracies," *Physical Review B* 99 (2019): 180101, https://link.aps.org/doi/10.1103/PhysRevB.99.180101.

22. H. Qin, Z. Su, M. Liu, et al., "Arbitrarily Polarized Bound States in the Continuum with Twisted Photonic Crystal Slabs," *Light: Science & Applications* 12, no. 1 (2023): 66, https://doi.org/10.1038/s41377-023-01090-w.

23. C. Huang, C. Zhang, S. Xiao, et al., "Ultrafast Control of Vortex Microlasers," *Science* 367, no. 6481 (2020): 1018–1021, https://www.science.org/doi/abs/10.1126/science.aba4597.

24. B. Wang, W. Liu, M. Zhao, et al., "Generating Optical Vortex Beams by Momentum-Space Polarization Vortices Centered at Bound States in the Continuum," *Nature Photonics* 14, no. 10 (2020): 623–628, https://doi.org/10.1038/s41566-020-0658-1.

25. M. Notomi, "Topology in Momentum Space Becomes Real," *Nature Photonics* 14, no. 10 (2020): 595–596, https://doi.org/10.1038/s41566-020-0693-y.

26. I. Meglinski, I. Lopushenko, A. Sdobnov, and A. Bykov, "Phase Preservation of Orbital Angular Momentum of Light in Multiple Scattering Environment," *Light: Science & Applications* 13, no. 1 (2024): 214, https://doi.org/10.1038/s41377-024-01562-7.

27. H. Zhong, Y. Yu, Z. Zheng, et al., "Ultra-Low Threshold Continuous-Wave Quantum Dot Mini-BIC Lasers," *Light: Science & Applications* 12, no. 1 (2023): 100, https://doi.org/10.1038/s41377-023-01130-5.

28. Y. Zeng, G. Hu, K. Liu, Z. Tang, and C.-W. Qiu, "Dynamics of Topological Polarization Singularity in Momentum Space," *Physical Review Letters* 127 (2021): 176101, https://link.aps.org/doi/10.1103/PhysRevLett.127.176101.

29. Y. Zhang, A. Chen, W. Liu, et al., "Observation of Polarization Vortices in Momentum Space," *Physical Review Letters* 120 (2018): 186103, https://link.aps.org/doi/10.1103/PhysRevLett.120.186103.

30. W. Liu, B. Wang, Y. Zhang, et al., "Circularly Polarized States Spawning from Bound States in the Continuum," *Physical Review Letters* 123 (2019): 116104, https://link.aps.org/doi/10.1103/PhysRevLett.123.116104.

31. B. Zhen, C. W. Hsu, L. Lu, A. D. Stone, and M. Soljačić, "Topological Nature of Optical Bound States in the Continuum," *Physical Review Letters* 113 (2014): 257401, https://link.aps.org/doi/10.1103/PhysRevLett.113.257401.

32. X. Zhang, Y. Liu, J. Han, Y. Kivshar, and Q. Song, "Chiral Emission from Resonant Metasurfaces," *Science* 377, no. 6611 (2022): 1215–1218, https://www.science.org/doi/abs/10.1126/science.abq7870.

33. J. Chen, Z. Chen, Z. Zhou, Y. Lu, and J. Kou, "Spin-Dependent Edge Detection and Imaging Enabled by Optical Circularly Polarized States," *Light: Advanced Manufacturing* 6, no. LAM2024060066 (2025): 62, https://www.light-am.com//article/id/44f27b1a-9c17-4a0c-8a80-9fb8d81cdcdd.

34. D. Xing, M.-H. Chen, Z. Wang, B.-W. Lin, H. Tabata, and J.-J. Delaunay, "Chiral Lasing Emission from a Simple Two-Unit Supercell Metasurface," *Laser & Photonics Reviews* 19, no. 20 (2025): e00530, https://onlinelibrary.wiley.com/doi/abs/10.1002/lpor.202500530.

35. X. Wang, J. Wang, X. Zhao, L. Shi, and J. Zi, "Realizing Tunable Evolution of Bound States in the Continuum and Circularly Polarized Points by Symmetry Breaking," *ACS Photonics* 10, no. 7 (2023): 2316–2322, https://doi.org/10.1021/acsphotonics.2c01522.

36. S. Fan, W. Suh, and J. D. Joannopoulos, "Temporal Coupled-Mode Theory for the Fano Resonance in Optical Resonators," *Journal of the Optical Society of America A: Optics, Image Science, and Vision* 20, no. 3 (2003): 569–572, https://opg.optica.org/josaa/abstract.cfm?URI=josaa-20-3-569.

37. A. Overvig, S. A. Mann, and A. Alù, "Spatiotemporal Coupled-Mode Theory for Nonlocal Metasurfaces," *Light: Science & Applications* 13, no. 1 (2024): 28, https://doi.org/10.1038/s41377-023-01350-9.

38. S. Fan and J. D. Joannopoulos, "Analysis of Guided Resonances in Photonic Crystal Slabs," *Physical Review B* 65 (2002): 235112, https://link.aps.org/doi/10.1103/PhysRevB.65.235112.

Supporting Information

Additional supporting information can be found online in the Supporting Information section.

Supporting Information